Malaria-driven expansion of adaptive-like functional CD56-negative NK cells correlates with clinical immunity to malaria

Prasanna Jagannathan (prasj@stanford.edu)
Stanford University https://orcid.org/0000-0001-6305-758X

Maureen Ty
Stanford University

Shenghuan Sun
University of California, San Francisco

Perri Callaway
University of California, San Francisco

John Rek
Infectious Diseases Research Collaboration

Kathleen Dantzler
Stanford University

Kattria van der Ploeg
Stanford University https://orcid.org/0000-0002-3183-3190

Jason Nideffer
Stanford University

Zicheng Hu
University of California, San Francisco

Sandy Klemm
Stanford University

William Greenleaf
Stanford University https://orcid.org/0000-0003-1409-3095

Michele Donato
Stanford University School of Medicine https://orcid.org/0000-0002-9968-6027

Stephen Tukwasibwe
Infectious Diseases Research Collaboration

Emmanuel Arinaitwe
Infectious Dieases Research Collaboration

Felistas Nankya
Infectious Diseases Research Collaboration

Kenneth Musinguzi

Infectious Diseases Research Collaboration
Dean Andrew
QIMR Berghofer Medical Research Institute
Lauren de la Parte
Stanford University
Diego Mori
Stanford University
Saki Takahashi
University of California, San Francisco https://orcid.org/0000-0001-5413-5507
Isabel Rodriguez-Barraquer
UCSF
Bryan Greenhouse
UCSF
Catherine Blish
Stanford University https://orcid.org/0000-0001-6946-7627
Paul Utz
Stanford University School of Medicine https://orcid.org/0000-0003-1181-1565
Purvesh Khatri
Stanford University https://orcid.org/0000-0002-4143-4708
Grant Dorsey
University of California San Francisco
Moses Kamya
Infectious Dieases Research Collaboration
Michelle Boyle
QIMR-Berghofer https://orcid.org/0000-0002-0268-232X
Margaret Feeney
Unviersity of California San Francisco
Isaac Ssewanyana
Infectious Diseases Research Collaboration

Article

Keywords:

Posted Date: November 7th, 2022

DOI: https://doi.org/10.21203/rs.3.rs-1820334/v1

Malaria-driven expansion of adaptive-like functional CD56-negative NK cells correlates with clinical immunity to malaria

Maureen Ty[1], Shenghuan Sun[2*], Perri C. Callaway[3*], John Rek[4*], Kathleen D. Press[1*], Kattria van der Ploeg[1*], Jason Nideffer[1], Zicheng Hu[2], Sandy Klemm[5], William Greenleaf[5], Michele Donato[6], Stephen Tukwasibwe[4], Emmanuel Arinaitwe[4], Felistas Nankya[4], Kenneth Musinguzi[4], Dean Andrew[7], Lauren de la Parte[1], Diego Martinez Mori[1], Saki Takahashi[3], Isabel Rodriguez-Barraquer[3], Bryan Greenhouse[3], Catherine Blish[1,8], PJ Utz[1], Purvesh Khatri[6], Grant Dorsey[3], Moses Kamya[4,9], Michelle Boyle[7], Margaret Feeney[3,10], Isaac Ssewanyana[4], Prasanna Jagannathan[1,11,#]

[1]Department of Medicine, Stanford University

[2]Bakar Computational Health Sciences Institute, University of California, San Francisco

[3]Department of Medicine, University of California, San Francisco

[4]Infectious Diseases Research Collaboration, Kampala, Uganda

[5]Department of Genetics, Stanford University

[6]Institute for Immunity, Transplantation, and Infection, Stanford University

[7]Queensland Institute for Medical Research, Queensland, Australia

[8]Chan Zuckerberg Biohub, San Francisco, CA

[9]Department of Medicine, Makerere University, Kampala, Uganda

[10]Department of Pediatrics, University of California, San Francisco

[11]Department of Microbiology and Immunology, Stanford University

*These authors contributed equally

[#]Correspondence to Prasanna Jagannathan, 240 Pasteur Drive Room 3456, Stanford CA 94305

Abstract:

Natural Killer (NK) cells likely play an important role in immunity to malaria, but whether repeated malaria modifies the NK cell response remains unclear. Here, we comprehensively profiled the NK cell response in a cohort of 264 Ugandan children. Repeated malaria exposure was associated with expansion of an atypical, $CD56^{neg}$ population of NK cells that differed transcriptionally, epigenetically, and phenotypically from $CD56^{dim}$ NK cells, including decreased expression of PLZF and the Fc receptor γ chain, increased histone methylation, and increased protein expression of LAG-3, KIR and LILRB1. $CD56^{neg}$ NK cells were highly functional, displaying greater antibody dependent cellular cytotoxicity than $CD56^{dim}$ NK cells, and higher frequencies of these cells were associated with protection against symptomatic malaria and high parasite densities. Importantly, following marked reductions in malaria transmission, frequencies of these cells rapidly declined, suggesting that continuous exposure to malaria is required to maintain this modified, adaptive-like NK cell subset.

Introduction

Plasmodium falciparum (Pf) malaria resulted in an estimated 240 million cases and 624,000 deaths in 2020, with rising morbidity observed in several highly endemic countries exacerbated by the COVID-19 pandemic[1]. The burden of disease falls mainly on young African children, with 77% of deaths reported in African children less than 5 years of age. With increasing age and repeated malaria episodes, children eventually gain protection against severe disease, followed by protection against symptomatic illness. This age- and exposure- dependent clinical immunity is comprised of two distinct components: “anti-parasite” immunity, or partial control of blood-stage parasite densities, and “anti-disease” immunity, or the ability to tolerate higher parasite densities without fever[2]. However, clinical immunity is short-lived, and the precise determinants driving these distinct components of naturally acquired anti-malarial immunity remain poorly understood[3].

Although malaria-specific antibodies likely play a key role in clinical immunity through both binding inhibition and Fc-dependent antibody effector functions[4, 5, 6, 7, 8], the role of the cellular immune response in clinical immunity is less clear. Innate immune cells can recognize and respond to *Plasmodium* parasites[9, 10, 11], but pathogen-induced production of inflammatory cytokines by these cells has also been implicated in the pathogenesis of symptomatic and severe malaria[9, 12]. The development of naturally acquired immunity likely involves the careful regulation of the innate immune response to limit the negative consequences of inflammation while partially controlling parasitemia. Indeed, recent studies have suggested that repeated exposure to malaria may modify several innate immune cells[13, 14, 15, 16, 17], potentially through transcriptional and epigenetic reprogramming[15, 18]. Whether malaria-induced innate immune modulation plays a role in driving and/or maintaining naturally acquired immunity is unknown.

Natural killer (NK) cells have increasingly been recognized as playing a key role in the host immune response to malaria through both direct parasite recognition[19, 20] and antibody-dependent cellular cytotoxicity[8] (reviewed in[21]). These cells have traditionally been divided into subsets based on expression of CD56 and CD16, with $CD56^{dim}CD16^{+}$ NK cells typically comprising the majority of the NK population in peripheral blood, although the complexity and diversity of NK cell subsets has only recently been interrogated using single cell approaches[22, 23, 24]. Recently, a subset of $CD56^{dim}$ NK cells with low expression of the transcription factor promyelocytic leukemia zinc finger (PLZF) and the signaling Fc receptor γ-chain (FcRγ) were found to have enhanced, antibody-dependent cellular cytotoxicity against *Pf* infected red blood cells and were associated with resistance to symptomatic malaria in Malian children[25]. It remains unclear whether repeated malaria drives expansion of this "adaptive-like" NK cell subset or whether these cells are maintained stably in the absence of continuous exposure to malaria parasites. In addition, some reports have also described a subset of $CD56^{neg}$ $CD16^{+}$ NK cells that are expanded in the context of chronic viral infections such as HIV[26], HCV[27], as well as among patients with acute myelogenous lymphoma[28] and malaria-exposed African children with EBV-related Burkitt's lymphoma[29]. Given a reduced capacity of these cells to produce cytokines in response to stimulation, some suggest these cells may represent a dysfunctional and/or exhausted phenotype[28, 30]. Whether $CD56^{neg}$ NK cells expand following repeated malaria, have functional capabilities, and/or play a role in clinical immunity to malaria, is unknown.

In this study, we characterized the NK cell response among 264 children followed in the East African International Centers of Excellence in Malaria Research (ICEMR) cohorts in Eastern Uganda. We utilized multiparameter flow cytometry, cellular indexing of transcriptomes and epitopes by sequencing (CITE-Seq), Epigenetic profiling using cytometry by time of flight (EpiTOF) and assay for transposase-accessible chromatin using sequencing (ATAC-Seq), along with functional assays, to comprehensively profile the NK cell response. We demonstrate that

repeated malaria exposure is associated with expansion of highly functional CD56^{neg} NK cells that strongly correlate with acquisition of clinical immunity to malaria; however, in the absence of continuous malaria exposure, frequencies and function of these cells rapidly decline.

Results

Increasing exposure to malaria is associated with higher frequencies of CD3^{-} CD7^{+} CD56^{neg} NK cells

We first analyzed circulating NK cell populations from PBMC collected in 2013 among 45 children ages 3-7 living in two districts in Eastern Uganda with very different malaria transmission intensities: Jinja, with an estimated annual entomological inoculation rate (aEIR) of 2.8 infectious bites per person per year, and Tororo, with an aEIR of 310 infectious bites per person year[31]. Nearly all children in this cohort were HCMV positive at the time of sampling (**Supplemental Table 1**). NK cells were phenotypically defined as CD3^{-}, CD14^{-}, CD19^{-}, CD7+ cells and classified by the expression of CD56 and CD16 into three subsets: CD56^{bright} (CD56+ CD16-), CD56^{dim} (CD56^{dim} CD16+) and CD56^{neg} (CD56^{neg} CD16+) (**Fig 1A, Supplemental Figure 1**). Children living in highly endemic Tororo district had significantly lower frequencies of CD56^{dim} NK cells, and higher frequencies of CD56^{neg} NK cells, than age-matched children living in Jinja (**Fig 1B, Supplemental Table 1**). Percentages of CD56^{neg} NK cells positively correlated with household-level aEIR, a direct measurement of household exposure to *Pf* infective mosquitoes (**Fig 1C**). We also correlated frequencies of NK cell subsets with age, a surrogate for cumulative malaria exposure in high transmission settings, among a larger Tororo cohort of 242 children ages 6 months to 10 years (**Supplemental Table 2**). We found that increasing age was associated with increasing frequencies of CD56^{neg} NK cells, and decreasing frequencies of CD56^{dim} NK cells (**Fig 1D**). Together these data suggest that CD56^{neg} NK cells are increased in children repeatedly exposed to malaria.

Figure 1

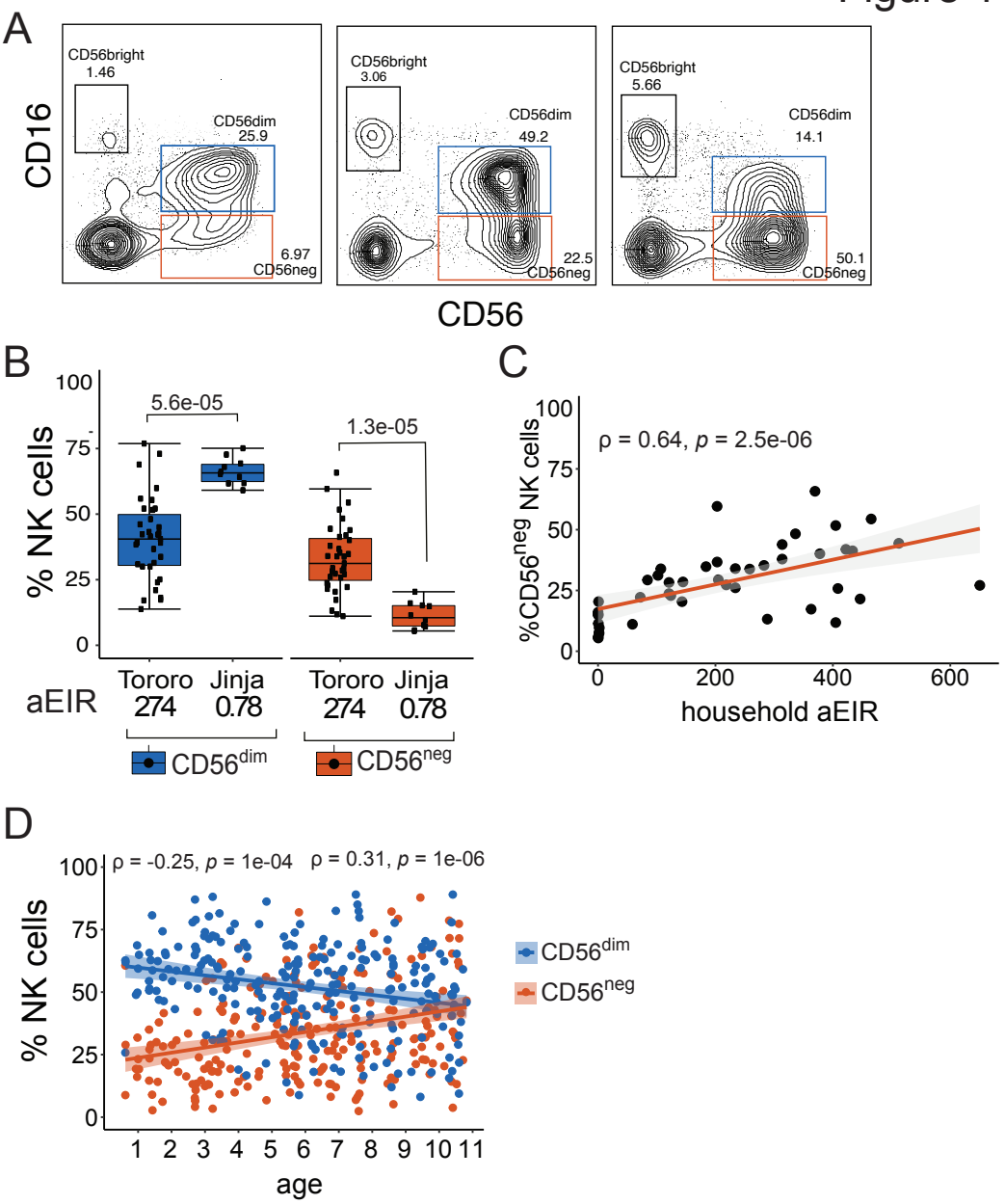

Figure 1: Ugandan children living in high transmission settings have high frequencies of atypical CD56^{neg} NK cells. (A) Representative flow cytometry plots of CD3^{-} CD14^{-} CD19^{-} CD7^{+} NK cells from three children, as defined by CD56 and CD16. (B) Percentages of CD56^{dim} and CD56^{neg} NK cells from children ages 3-7 years in Tororo (n=35) and Jinja (n=10). Household annual Entomological Inoculation Rate (aEIR) is an estimate of the number of infective bites received in the year prior to sampling across each cohort, as measured via CDC light traps (see methods). (C). Correlation between CD56^{neg} NK cells and measured household aEIR among children assayed in (B). (D) Correlation between NK cell frequencies and age among 242 Tororo children ages 0.6 to 11 years. P-values shown above box plots are calculated using Wilcoxon signed rank test, while the rho (ρ) and p-values associated with the scatterplots are calculated using Spearman's correlation. Shaded areas represent 95% confidence interval of best fit regression line. All samples were collected in 2013, see Supplemental Table 1 and 2 for patient characteristics.

Single cell RNA sequencing reveals that CD56^{neg} NK cells have transcriptional features of both "adaptive" and "exhausted" NK cells

To further characterize NK cells at the single cell level, we used Cellular Indexing of Transcriptomes and Epitopes by Sequencing (CITE-Seq), a method of single cell RNA sequencing that simultaneously assesses DNA-barcoded antibodies against cell surface proteins. Peripheral blood mononuclear cells from 10 independent Tororo participant samples were analyzed (n=60,381 total cells, **Supplemental Table 3**). Unsupervised clustering of RNA transcripts using uniform manifold approximation and projection (UMAP) revealed that NK cells cluster near T cells, with CD8^{+} T cells as the closest neighbors (**Fig 2A**). Using cell surface protein tags for CD56 and CD16, we identified 3 distinct cell subsets within the CD19-, CD3-, CD14- CD7+ NK cell population (**Fig 2B)** and visualized these cell populations on the RNA UMAP projection. CD56^{dim} and CD56^{neg} NK cells were both identified in the same NK cell RNA cluster, suggesting transcriptional similarities between these subsets (**Fig 2C, Supplemental Figure 2**). However, we also identified gene transcripts differently enriched in each subset (**Fig 2D**). In comparison to CD56^{dim} NK cells, CD56^{neg} cells had significantly lower expression of *ZBTB16*, which encodes the transcription factor PLZF, and *FCER1G,* which encodes the FcRγ signaling receptor (**Fig 2E** top row). Conversely, CD56^{neg} NK cells had higher expression of *BC11B*, a transcription factor recently shown to repress PLZF[32] (**Fig 2E**). Expression of PLZF and FcRγ are decreased in adaptive-like NK cells[24], a pattern that has also been associated with enhanced antibody-dependent cellular cytotoxicity[25]. CD56^{neg} NK cells also had lower expression of genes encoding the cell surface markers *KLRB1* (CD161) and *KLRF1* (NKp80), and higher expression of *CD3G*, than CD56^{dim} NK cells, also consistent with an adaptive-like NK cell phenotype[24, 33]. Interestingly, CD56^{neg} NK cells had lower expression of *IL18RAP*, which encodes the IL18 receptor accessory protein and mediates IL18-dependent signal transduction

and downstream NF-κB activation and IFNγ induction[34]. CD56^{neg} NK cells also had higher expression of *LAG3*, a checkpoint inhibitor which is induced by type I IFN[35] and chronic *in vitro* stimulation[36], and is a negative regulator of cytokine production in mature NK cells, suggestive of an exhausted phenotype[36, 37]. Expression of killer cell immunoglobulin-like receptor (KIR) genes were similar between CD56^{dim} and CD56^{neg} NK cells, consistent with another published report[38], although KIR genes were not well represented in the dataset (**Fig 2E** bottom row). Together, these data suggest that CD56^{neg} NK cells from malaria-exposed Ugandan children have transcriptional features suggestive of both adaptive-like and exhausted NK cells.

Figure 2

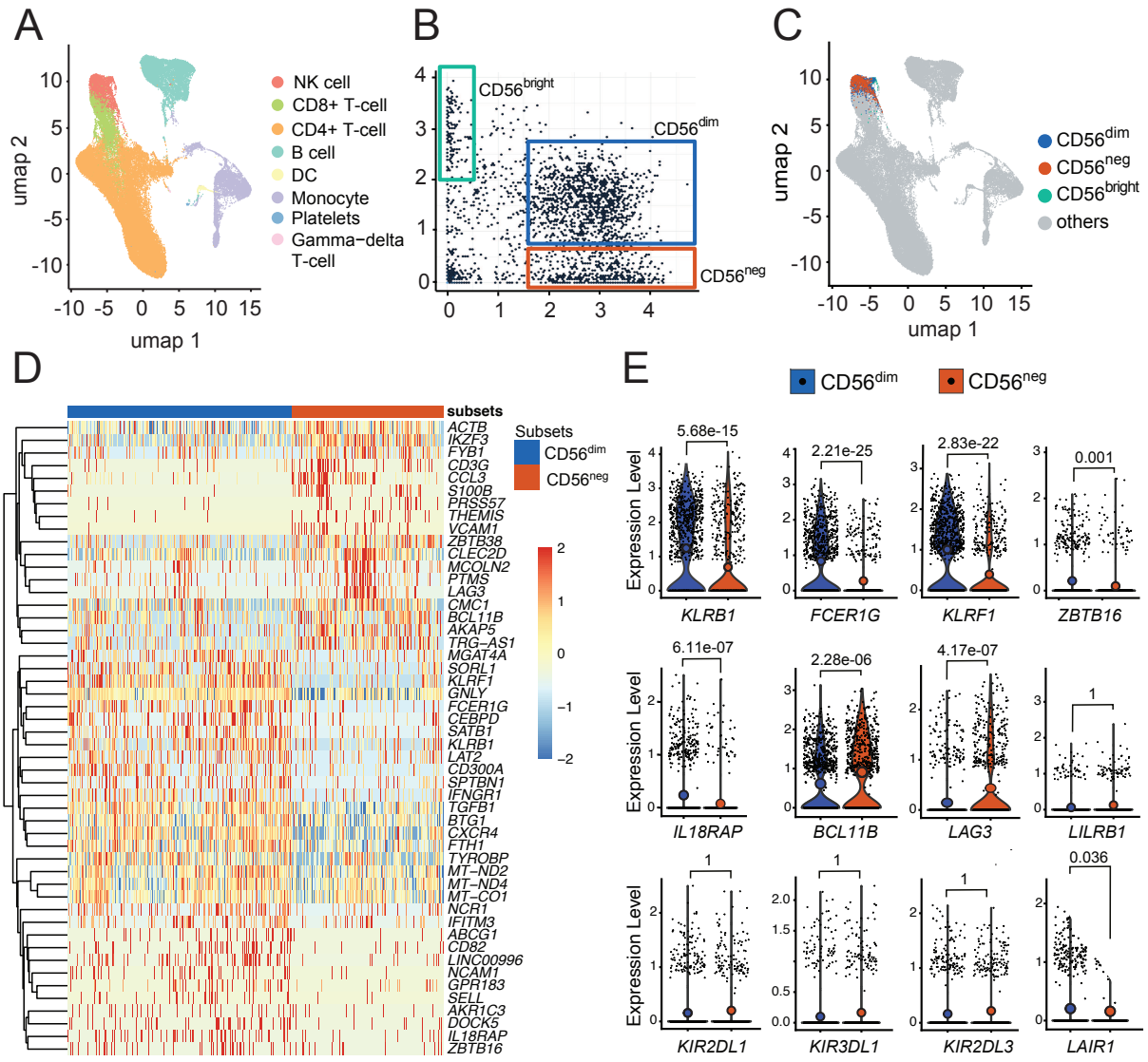

Figure 2: Single-cell RNA Sequencing of NK cells reveal transcriptional similarities and differences between CD56dim and CD56neg NK cells. **(A)** Gene transcripts of n=60381 PBMCs were clustered using Leiden algorithm and visualized in two dimensions with UMAP. **(B)** Gating of NK cell subsets as defined by surface marker expression of CD16 (x-axis) and CD56 (y-axis). **(C)** NK cells subsets classified by **(B)** superimposed with UMAP gene transcript data. $CD56^{dim}$ transcripts are in blue, $CD56^{neg}$ in red, $CD56^{bright}$ in green and non-NK cell transcripts are in grey. **(D)** Heatmap showing top 50 genes differentially expressed by $CD56^{dim}$ and $CD56^{neg}$ NK cells. **(E)** Representative violin plots comparing gene transcripts between $CD56^{dim}$ and $CD56^{neg}$ NK cells. P values obtained from likelihood ratio tests as implemented in the Seurat R package. Samples are from 10 individuals, see supplemental table 3 for patient characteristics.

CD56^{neg} NK cells from Ugandan children express higher levels of LILRB1 and KIRs and differ epigenetically from CD56^{dim} NK cells

Following transcriptional assessment, we next compared protein expression between CD56^{dim} and CD56^{neg} subsets from samples collected from 35 Tororo children (**Supplemental Table 4**). We initially focused on markers that have been implicated in NK cell differentiation[39] and/or adaptive NK cells[40] using flow cytometry, including cell surface receptors LILRB1 (CD85J), NKG2A, NKG2C, and CD57 as well as intracellular signaling receptor FcRy. Consistent with our gene expression data, CD56^{neg} NK cells in Tororo children had significantly reduced expression of FcRγ compared with CD56^{dim} NK cells. In addition, CD56^{neg} NK cells also had reduced protein expression of NKG2A, CD57, and NKG2C, but higher levels of LILRB1, compared with CD56^{dim} NK cells (**Fig3A, Supplementary Figure 3**). We examined the combination of these markers, and found that majority of the CD56^{neg} NK cells are LILRB1+, FcRγ-, NKG2A- and CD57-, while CD56^{dim} NK cells are most likely to be FcRγ+ and NKG2A+, but LILRB1- and CD57- (**Fig3B**). This phenotypic description of CD56^{neg} NK cells is consistent with similar cell populations within the context of chronic viral infections such as HIV[26]. Regarding KIRs, KIR2DL1 and 3DL1 were recently shown to be present in >98% of Ugandans studied in the ICEMR cohorts[41]. Cell surface expression of KIR2DL1 were similar between CD56^{neg} cells and CD56^{dim} cells, consistent with gene expression data. However, flow cytometric analysis revealed significantly greater cell surface expression of the KIRs KIR3DL1 and KIR2DL2/L3/S2 in CD56^{neg} NK cells compared to CD56^{dim} cells (**Fig3C**), consistent with other reports which have observed increased KIR protein expression on CD56^{neg} NK cells[26]. Additionally, we confirmed other differences seen in our gene expression data, including greater LAG3 expression and lower granulysin, among CD56^{neg} compared with CD56^{dim} cells (**Fig3D**).

Epigenetic differences in NK cells, including both genome-wide DNA hypo- and hypermethylation, have been previously shown to differentiate NK cell subsets, including adaptive NK cells[36, 40]. We compared global histone modifications at the single cell level between $CD56^{dim}$ and $CD56^{neg}$ NK cells using epigenetics by time of flight (EpiTOF), as global histone modifications have previously been shown to differentiate $CD56^{bright}$ and $CD56^{dim}$ NK cells[42]. Compared with $CD56^{dim}$ NK cells, $CD56^{neg}$ cells had greater abundance of a number of methylation marks, including di- and trimethylation of histone H3 lysine 4 (H3K4me2 and H3K4me3, **(Fig 3E)**), marks which are associated with gene expression in mature, aging cells[43]. Taken together these data suggest that $CD56^{neg}$ NK cells in malaria-exposed Ugandan children have phenotypic and epigenetic features of mature, adaptive-like NK cells that differentiate them from $CD56^{dim}$ cells.

Figure 3

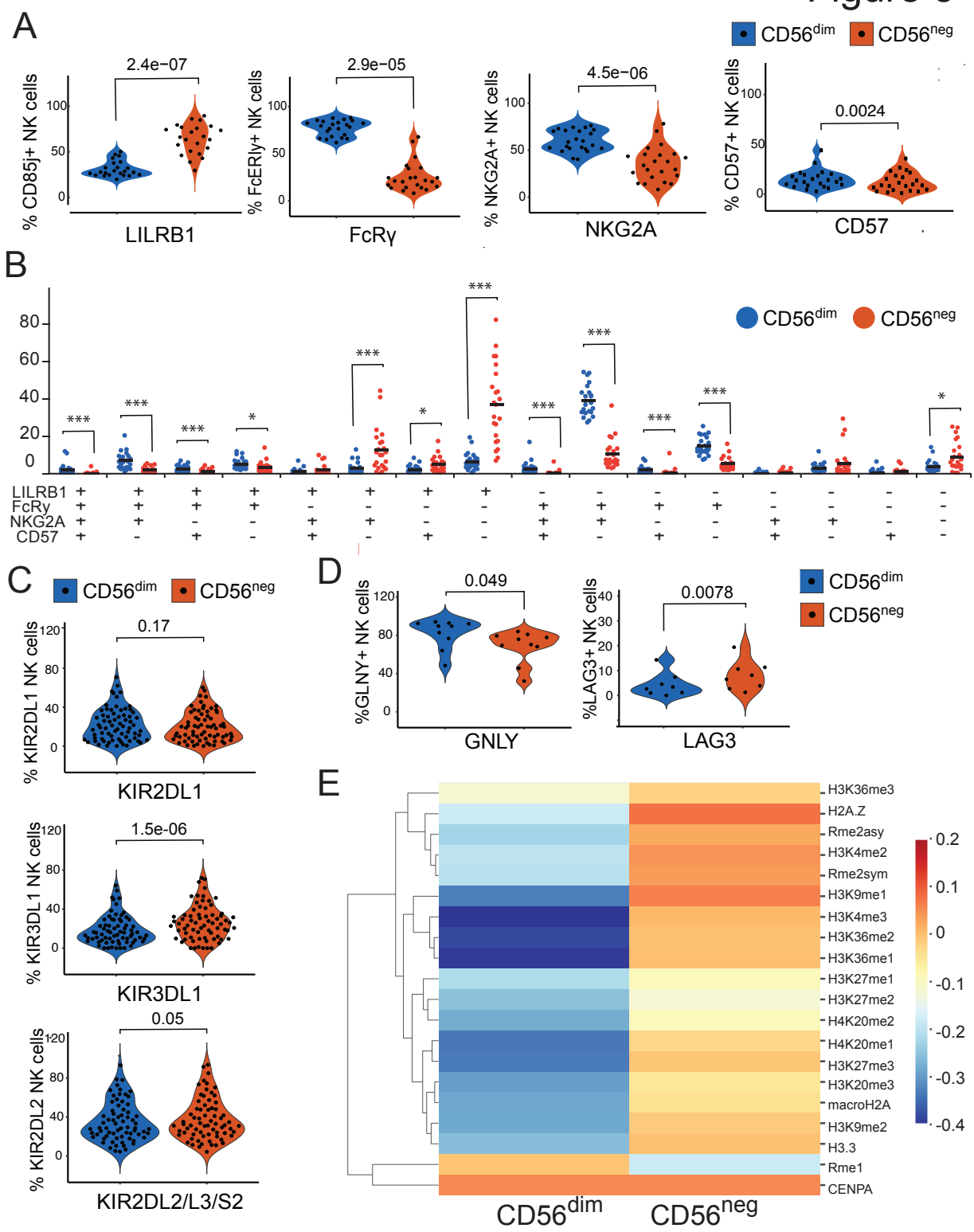

Figure 3: Cellular phenotyping reveals CD56^{neg} NK cells to have a mature phenotype. NK cells were gated for positive staining for LILRB1, FcRγ, NKG2A and CD57. **(A)** Frequencies of cells are shown in

violin plots. **(B)** Proportions of cells expressing all four possible marker combinations are shown in dot plots. **(C & D)** Percentages of NK cells expressing KIRs**,** Granulysin and LAG3. **(E)** Heatmap comparing distinct histone modifications between $CD56^{dim}$ and $CD56^{neg}$ NK cells as measured by EpiTOF from 36 participant samples. P-values shown above violin and dot plots are calculated using Wilcoxon matched-pairs signed rank test. See Supplemental Table 4 for number of samples and patient characteristics, and Supplemental Figures 1 and 3 for gating strategies.

$CD56^{neg}$ NK cells display greater antibody-dependent cellular cytotoxicity (ADCC) than $CD56^{dim}$ NK cells

Having demonstrated that $CD56^{neg}$ NK cells were transcriptionally, phenotypically, and epigenetically distinct from $CD56^{dim}$ NK cells, we next compared their functional abilities. Following a short *in vitro* stimulation with *Plasmodium falciparum* infected red blood cells (iRBCs), neither $CD56^{dim}$ nor $CD56^{neg}$ NK cells produced significant amounts of IFNγ (**Fig 4A**). However, following IL-12/IL-15/IL-18 stimulation, we observed that $CD56^{neg}$ NK cells produced significantly less IFNγ in comparison to $CD56^{dim}$ cells. This result was expected given CITE-Seq data showing decreased expression of *IL18RAP* on $CD56^{neg}$ compared to $CD56^{dim}$ NK cells, and also consistent with prior reports suggesting that $CD56^{neg}$ NK cells are unable to respond robustly to cytokine stimulation[30].

We next tested whether there were differences between $CD56^{dim}$ or $CD56^{neg}$ NK cells in response to antibody-opsonized target cells. We stimulated PBMC obtained from Ugandan children with a range of $CD56^{neg}$ and $CD56^{dim}$ NK cell frequencies with iRBCs alone, iRBC incubated with plasma pooled from either malaria-naïve adults or immune Ugandan adults, or, as a positive control, iRBCs incubated with anti-RBC antibodies. In response to iRBC incubated with plasma from immune Ugandan adults, $CD56^{neg}$ NK cells produced significantly more IFNγ and had greater degranulation (as measured by CD107a) in comparison with $CD56^{dim}$ NK cells, suggesting a heightened capacity to perform ADCC **(Fig 4B and C)**. Following stimulation with iRBCs alone or iRBC treated with plasma from malaria-naïve adults, neither $CD56^{dim}$ nor $CD56^{neg}$ NK produced IFNγ or degranulated **(Fig 4B and C)**, indicating the observed responses were truly antibody-dependent.

To determine whether malaria-specific NK cell degranulation was independent of other cells, we isolated NK cells from 15 Tororo children by magnetic purification and performed the same ADCC assay. Again, isolated NK cells degranulated more when stimulated with iRBC incubated with pooled plasma from Ugandan adults vs. iRBC incubated with US control plasma (**Fig 4D; Supplemental Figure 1 for gating strategy**). The majority of degranulating, $CD107a^{+}$ NK cells following stimulation with Ugandan plasma opsonized parasites were $FcR\gamma^{-}$, $LILRB1^{+}$, $NKG2A^{-}$ and $CD57^{-}$ (**Fig 4E**), which represent the major fraction of circulating $CD56^{neg}$ NK cells (**Fig 3B**). Other NK cell populations that degranulated also lacked expression of FcRγ (**Fig 4E**), including those that were $CD56^{dim}$, consistent with other studies showing that $FcR\gamma^{-}$ $CD56^{dim}$ NK cells show enhanced degranulation to antibody-coated targets[25, 44].

As an alternative measure of ADCC, we assessed the ability of NK cells to kill antibody-coated p815 cells. Following stimulation with antibody-coated p815 cells, we observed a strong positive correlation between frequencies of $CD56^{neg}$ NK cells and p815 killing (**Fig 4F, Supplemental Figure 4**), which suggest that $CD56^{neg}$ NK cells are able to kill antibody opsonized targets. We further isolated NK cells and show that these cells are the main cell type that kill antibody opsonized p815 compared to PBMCs that were depleted of NK cells (**Figure 4G**). Taken together, these results demonstrate that malaria-induced $CD56^{neg}$ NK cells have enhanced ADCC capacity compared to $CD56^{dim}$ NK cells.

Figure 4

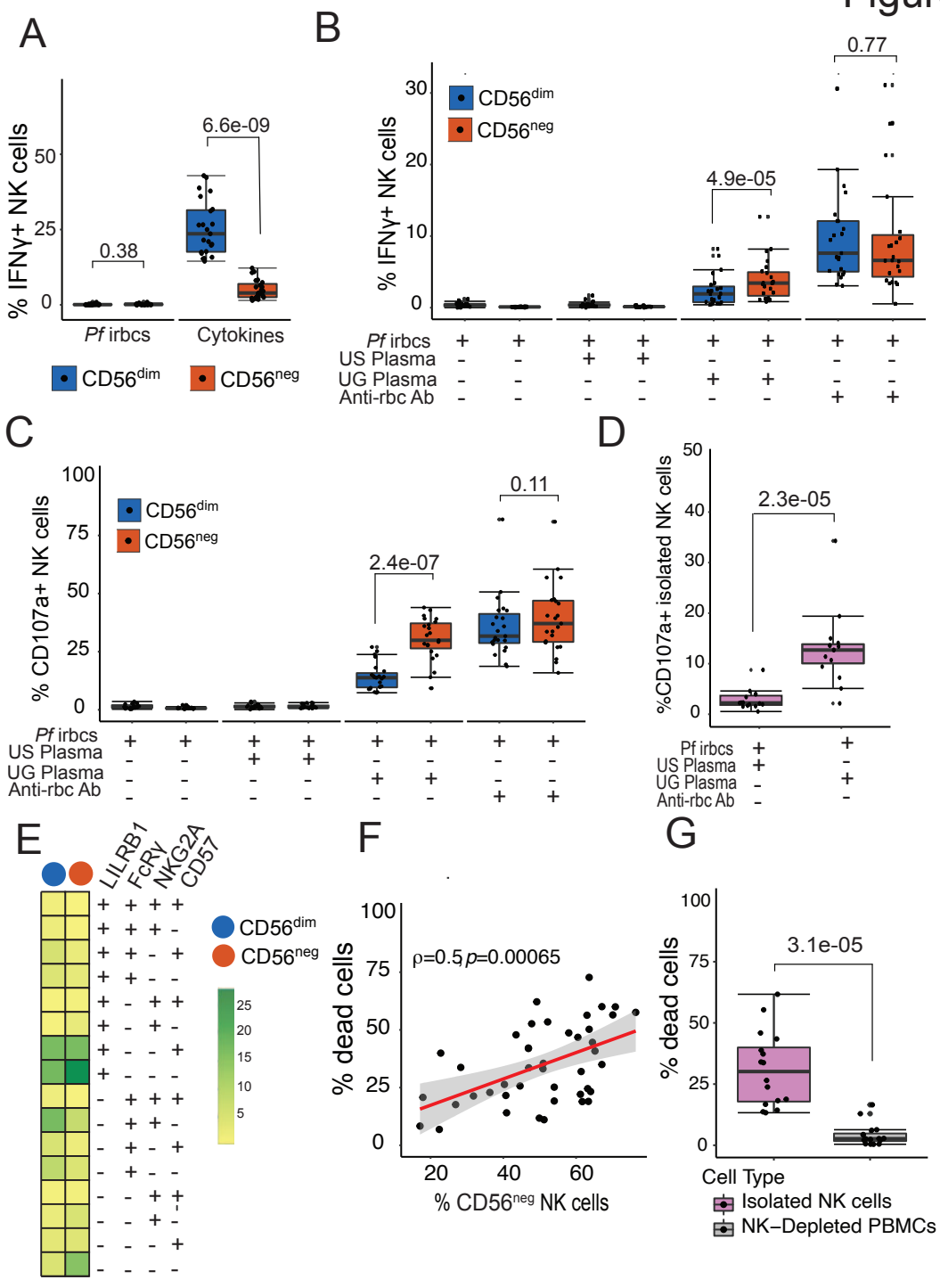

Figure 4: CD56^{neg} NK cells have an enhanced ability for antibody-dependent cellular cytotoxicity. **(A)** PBMCs were stimulated with iRBCs or cytokines: IL12 (2ng/ml), IL15 (10ng/ml) and IL18 (0.25ug/ml) for 4 hours, after which intracellular IFNγ was measured. **(B & C)** PBMCs were stimulated with either irbcs alone or opsonized with serum in a ratio of 2 PBMCs to 1 irbcs. **(B)** IFNγ was measured intracellularly. **(C)** NK cell degranulation was measured by CD107a expression. **(D)** Isolated NK cells were stimulated with iRBCs opsonized by either US or Ugandan serum and degranulation measured. **(E)** Heatplot showing NK

cells expressing specific markers, as detected by flow cytometry, degranulating in response to iRBCs opsonized by Ugandan serum. **(F)** Association between frequencies of $CD56^{neg}$ NK cells and corresponding percentage of dead opsonized p815 cells. **(G)** Isolated NK cells and NK-Depleted PBMCs were stimulated with opsonized p815s, after which the percentage of dead cells was measured by 7-AAD staining. P-values for box plots are calculated using Wilcoxon matched-pairs signed rank test, and rho (ρ) and p-value associated with the scatterplot is calculated using Spearman's correlation. See Supplemental Table 4 for number of samples and patient characteristics.

Higher frequencies of $CD56^{neg}$ NK cells are associated with protection against subsequent parasitemia and symptoms of malaria

To determine the clinical relevance of these observations, we looked for associations between NK cell percentages and a) parasite densities in the year following the cellular measurement (anti-parasite immunity), and b) the probability of symptoms given *Plasmodium* infection in the subsequent year (anti-disease immunity). Higher percentages of $CD56^{neg}$ NK cells were associated with significantly lower parasite densities in the year following the measurement, consistent with a role for $CD56^{neg}$ NK cells in anti-parasite immunity (**Fig 5A**). In contrast, higher percentages of $CD56^{dim}$ NK cells were associated with significantly higher parasite densities (**Fig 5A**). When considering the odds of symptoms given *Plasmodium* infection, higher percentages of $CD56^{neg}$ NK cells were also associated with a significantly lower odds of being symptomatic if infected (**Fig 5B, Supplemental Figure 5**). After adjustment for age and household aEIR, children in the highest tertile of $CD56^{neg}$ NK cells had a 71% lower odds of being symptomatic if infected in the subsequent year compared with children in the lowest tertile (adjusted odds ratio 0.29, 95% confidence interval 0.13-0.63, P=0.002, **Fig 5B**). In contrast, higher percentages of $CD56^{dim}$ NK cells were associated with higher odds of symptoms given infection (**Fig 5B, Supplemental Figure 5**). Together, these data suggest that higher frequencies of $CD56^{neg}$ NK cells, and inversion of the circulating $CD56^{dim}$ to $CD56^{neg}$ ratio, are strongly associated with both anti-parasite and anti-disease immunity to malaria in Ugandan children.

Figure 5

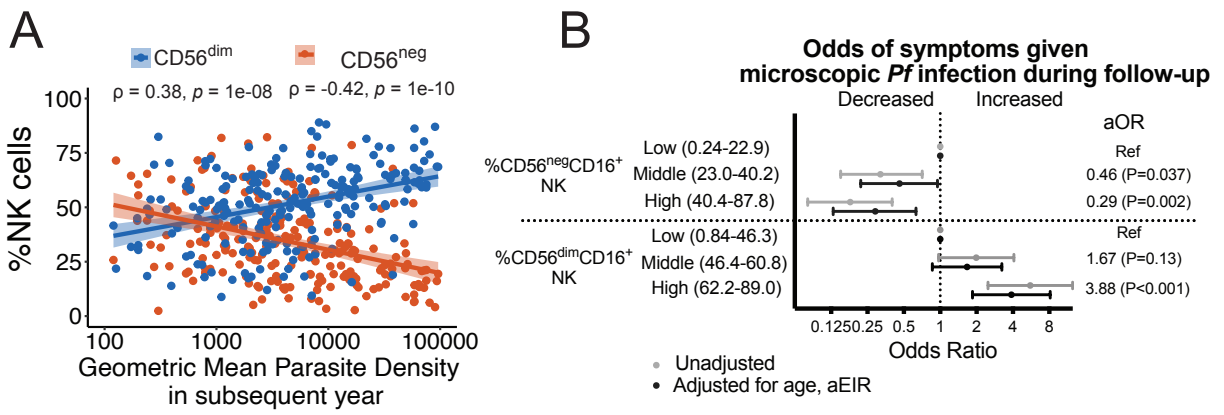

Figure 5: CD56^{neg} NK cells are associated with clinical malaria protection. Associations between CD56^{dim} and CD56^{neg} percentages and **(A)** geometric mean parasite densities in the subsequent year. Rho (ρ) and p-values associated with the scatterplot are calculated using Spearman's correlation. Shaded areas represent 95% confidence interval of best fit regression line. **(B)** Associations between CD56^{dim} and CD56^{neg} percentages and probability of symptoms given *Pf* parasitemia in the subsequent year (see Supplemental Figure 5 for smoothed relationships). Multilevel mixed effects linear models used to calculate odds of symptoms given microscopic *Pf* infection (B). Multivariate models adjusted for age and aEIR, and account for clustering by individual and household. Categories represent tertiles of NK response (n=80,81,81 per tertile). aOR: adjusted odds ratio. See Supplemental Table 2 for patient characteristics.

CD56neg NK cells decline in the setting of reduced malaria transmission

Having shown that functional CD56^{neg} NK cells are increased in children repeatedly exposed to malaria, we wanted to determine whether malaria exposure was required in order to maintain their phenotype and function. We took advantage of a natural experiment in our Tororo cohort where children were followed both before and after initiation of an indoor residual spraying of insecticide (IRS) campaign[45]. Prior to initiation of IRS in December 2014, malaria transmission was high and stable in Tororo[31]. Following initiation of IRS, malaria transmission, parasite prevalence and malaria incidence markedly declined, and by 2018, the burden of malaria was reduced to very low transmission levels (**Fig 6A**)[45]. We assessed the stability of NK cell phenotypes over time by performing longitudinal assessments in 15 Tororo children before (Aug-Nov 2013) and after (May-Oct 2015) the first round of IRS (**Supplemental Figure 6A**), and compared these with a group of 12 similarly aged children sampled in 2018, 4 years

after initiation of IRS when transmission was very low. Household aEIR among sampled participants declined from 277 in 2013 to 34 in 2015 to 1in 2018 (**Supplemental Table 5**). The percentage of $CD56^{neg}$ NK cells significantly decreased from the pre- to post-IRS period, with a concurrent increase of $CD56^{dim}$ cells (**Figure 6B and C**), and these percentages significantly correlated with household aEIR (**Supplemental Figure 6B**). Percentages of $CD56^{neg}$ NK cells were significantly lower in similarly aged children sampled in 2018, when transmission and malaria prevalence were markedly lower (**Figure 6B and C)**. Phenotypically, $CD56^{dim}$ NK cells did not significantly change with decreasing malaria transmission (**Fig 6C**). However, among $CD56^{neg}$ NK populations, we observed a significant decrease of the LILRB1+/-, FcRγ-, NKG2A-, CD57+/- NK cells that were predominant in 2013, as well as an increase in the LILRB1-, FcRγ+, NKG2A+ CD57- NK cells (**Figure 6D**).

Interestingly, the $CD56^{neg}$ populations that decreased were the two most predominant populations that degranulated when stimulated with antibody-opsonized parasites. To determine whether reductions in malaria transmission also altered epigenetic stability of NK cells, we measured chromatin accessibility of sorted NK cells collected in 2013 and 2015 using ATAC-Seq. We found that reductions in malaria transmission were associated with global changes in chromatin accessibility (**Fig 6E**). Specifically, accessibility to the promoter regions of the FcRγ, ZBTB16, KLRG1 and KLRD1 increased as malaria transmission declined (**Fig 6F**). These data suggest that loss of malaria exposure leads to changes in NK cell chromatin accessibility involving genes implicated in NK cell function.

Figure 6

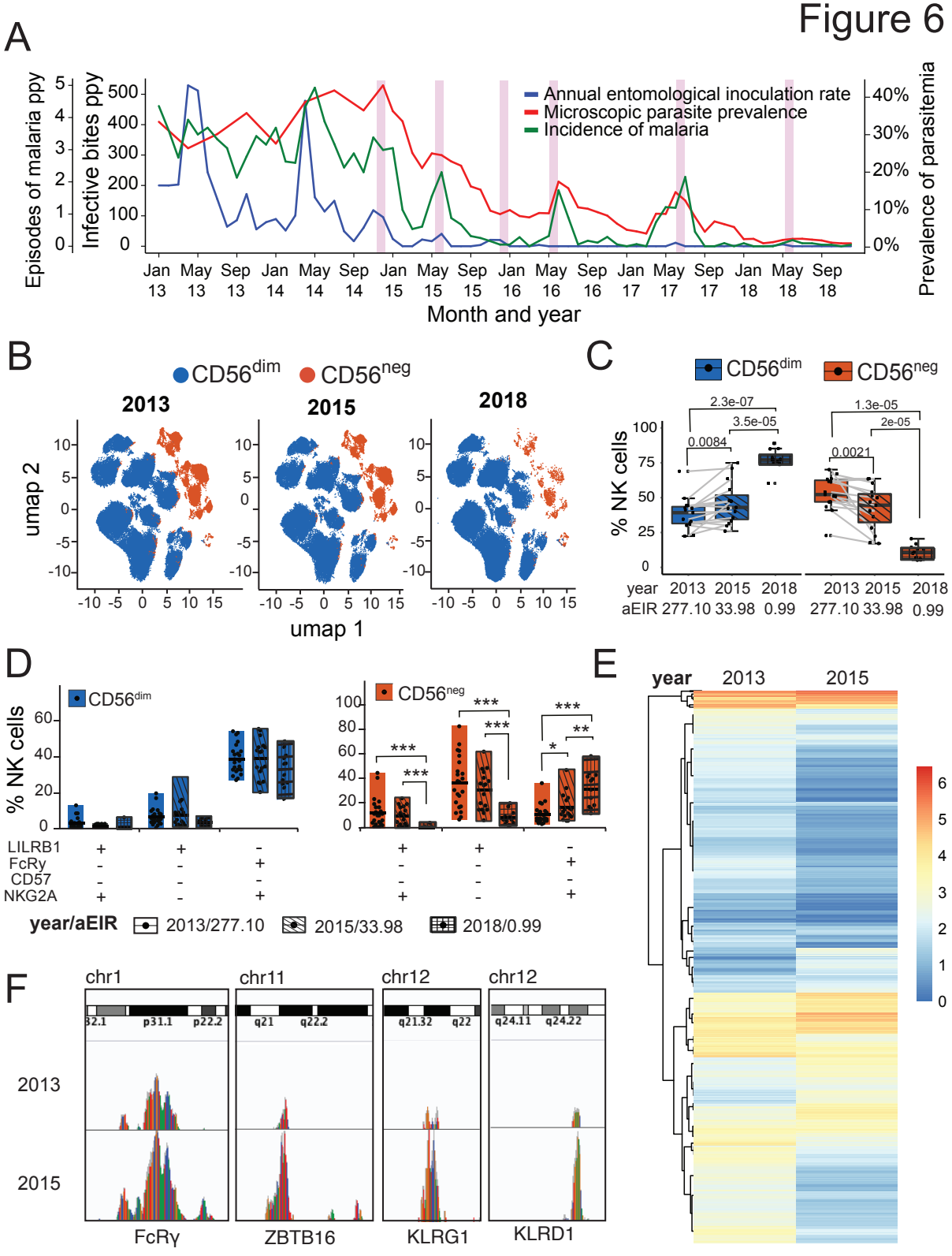

Figure 6: Decline of CD56^{neg} NK cell population following interruptions of malaria transmission. **(A)** Graph tracking measures of infection: infective bites per year (blue, middle y-axis), malaria incidence (green, left

y-axis), and parasitemia (red, right y-axis) from 2013 to 2018. Pink bars show repeated rounds of indoor residual spraying with insecticides. **(B)** Unsupervised clustering of $CD56^{dim}$ and $CD56^{neg}$ NK cells within individuals sampled in 2013 and 2015 (paired) and 2018 (unpaired, age-matched) and visualized by UMAP projections. **(C)** Frequencies of $CD56^{dim}$ and $CD56^{neg}$ NK cells over time (years) with decreasing malaria transmission. P **(D)** Proportion of $CD56^{dim}$ (blue) and $CD56^{neg}$ (red) NK cells expressing all possible marker combinations of CD85j, FcRy, NKG2A and CD57 plotted over time (years) as aEIR decreases. Clear box indicates 2013 (aEIR of 277.10), diagonal lined box indicates 2015 (aEIR of 33.98) and hatched box indicates 2018 (aEIR of 0.99). **(E)** ATAC-Seq heatmap showing differential accessibility of genes from FACS-sorted $CD3^{-}CD14^{-}CD19^{-}CD7^{+}$ NK cells obtained from a Tororo child sampled in 2013 and 2015 **(F)** ATAC-Seq genome tracks showing chromatin accessibility (peaks) at the FcRy, ZBTB16, KLRG1 and KLRD1 loci for 2013 and 2015 paired samples. P-values for box plots are calculated using Wilcoxon matched-pairs signed rank test.
Characteristics of participants sampled in this figure described in supplemental table 5.

Antibody-mediated cellular cytotoxicity function decline in $CD56^{neg}$ NK cell after decrease in malaria transmission

Finally, since we observed changes phenotypically and epigenetically in NK cells following declines in malaria transmission, we evaluated whether there were concomitant changes in NK cell function. We observed a significant decrease of total NK cell degranulation in response to Ugandan plasma opsonized iRBCs with decreasing malaria transmission (**Fig 7A, Supplemental Figure 6B**), with a stable response to a positive control, anti-RBC opsonized iRBC (**Fig 7A**). Looking more closely at cellular phenotypic subsets, we saw that $CD56^{neg}$ NK cells, but not $CD56^{dim}$ NK cells, exhibited significant reduction of degranulation in response to Ugandan plasma opsonized iRBCs (**Fig 7B**). Surprisingly, we observed a similar decline in $CD56^{neg}$, but not $CD56^{dim}$, degranulation in response to anti-RBC opsonized iRBC (**Fig 7C, Supplemental Figure 6C**). Furthermore, we observed a reduced ability to kill antibody-covered p815 cells post-IRS (**Fig 7D**). Collectively, these data are consistent with the hypothesis that ongoing malaria transmission is required to maintain both the frequency and effector function of $CD56^{neg}$ NK cells. Furthermore, the changing population of $CD56^{neg}$ NK cells in the setting of declining malaria transmission resulted in reduced ADCC activity of NK cells, including both degranulation and killing of target cells.

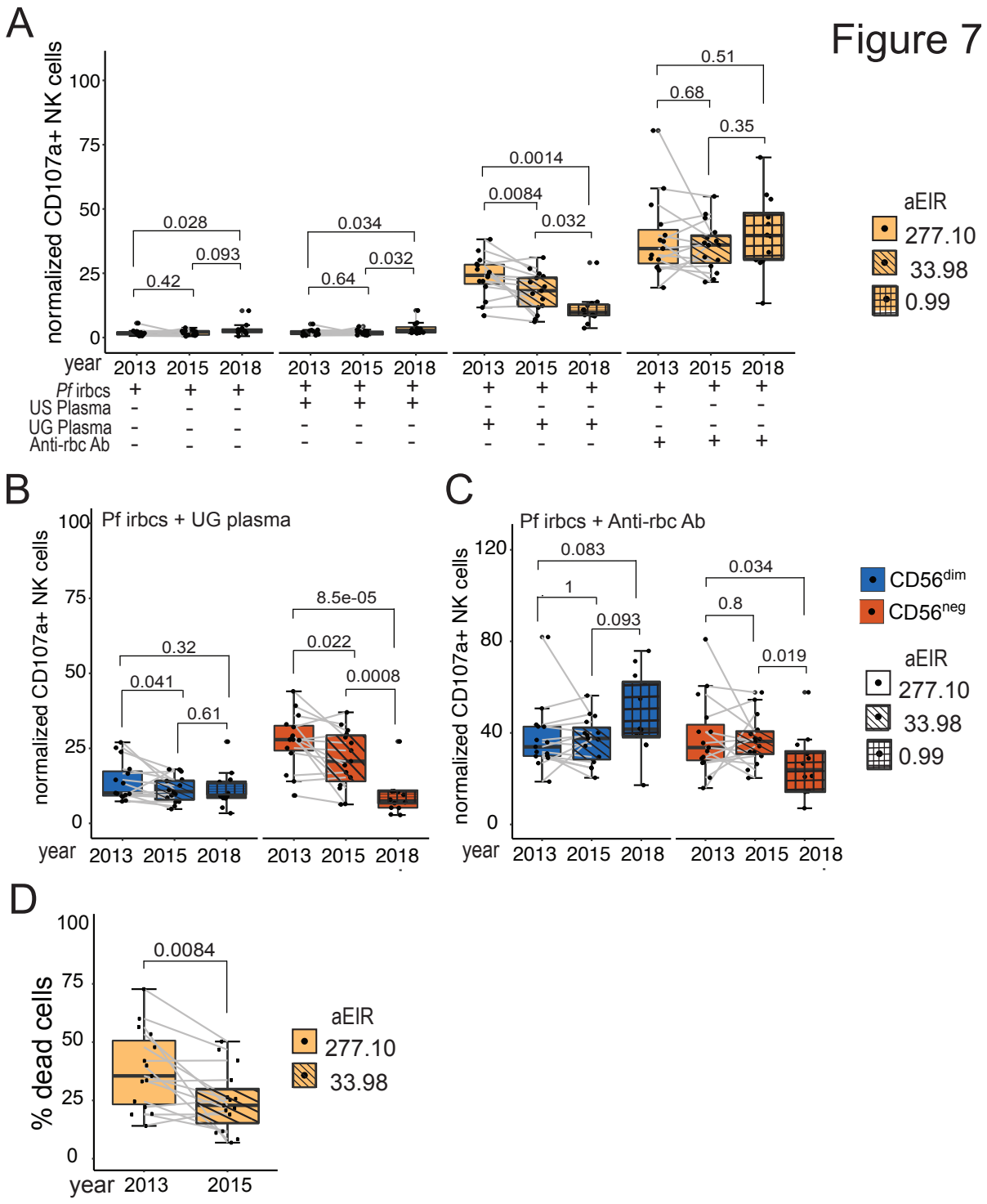

Figure 7: Reduction of ADCC by CD56^{neg} NK cells following decline of malaria transmission. **(A)** PBMCs were stimulated either with iRBCs alone or opsonized with serum. Degranulation was measured through the different years with decreasing aEIR. **(B & C)** PBMCs stimulated with iRBCs opsonized with Ugandan serum analyzed by NK cell subset. Degranulation by **(B)** CD56^{dim} and **(C)** CD56^{neg} NK cells was measured over time. **(D)** Killing of opsonized NK cells by PBMCs collected from 2013 and 2015. Clear box indicates 2013 with an aEIR of 258.3, diagonal lined box indicates 2015 with an EIR of 25.8 and

hatched box indicates 2018 with an aEIR of 0.43. P-values for box plots are calculated using Wilcoxon matched-pairs signed rank test. See Supplemental Table 5 for number of samples and patient characteristics.

Discussion

In this study, we characterized the NK cell response among children followed longitudinally across a range of malaria transmission intensities in Uganda. Children repeatedly exposed to malaria had increased frequencies of $CD56^{neg}$ NK cells that resembled $CD56^{dim}$ NK cells transcriptionally but with several key differences, including decreased expression of PLZF and FcRγ, global histone modifications, and increased protein expression of KIR3DL1 and KIR2DL2/L3/S2, LILRB1, and LAG-3. These $CD56^{neg}$ NK cells were highly functional, displaying greater malaria parasite-induced ADCC than $CD56^{dim}$ NK cells, and higher percentages of these cells were associated with both lower parasite densities and a lower probability of symptomatic disease upon subsequent *Plasmodium* infections. Importantly, following marked reductions in malaria transmission due to indoor residual spraying of insecticides, frequencies – and function - of $CD56^{neg}$ NK cells rapidly declined, suggesting that continuous exposure to malaria is required to maintain this modified, adaptive-like NK cell subset.

Although CD56 is the prototypical identifier of circulating human NK cells[46], our data suggest that $CD56^{neg}$ NK cells make up a significant fraction – and in many cases the majority – of circulating NK cells among children living in a high malaria transmission setting. $CD56^{neg}$ NK cells expressed CD7, which has previously been shown to differentiate NK cells from monocyte/DC like myeloid cells[47, 48], and transcriptional profiling of PBMC by CITE-Seq confirmed that $CD56^{neg}$ NK cells cluster similarly with $CD56^{dim}$ NK cells. Prior literature has suggested that $CD56^{neg}$ NK cells are dysfunctional and likely represent an exhausted phenotype, given that they have a reduced ability to produce cytokines in response to stimulation[28, 30]. We similarly observed that $CD56^{neg}$ cells in malaria-exposed children produce

less IFNγ in response to IL12/IL15/IL18 stimulation than CD56^{dim} NK cells. CD56^{neg} NK cells expressed lower levels of *IL18RAP*, which likely limits IL-18-mediated cellular activation[34], and higher levels of LAG-3, which likely negatively regulates cytokine production in these cells similar to its role in other NK cells[36]. Intriguingly we also observed that CD56^{neg} cells express high levels of the inhibitory receptor LILRB1. Recent studies have illuminated that a subset of *Pf* expressed RIFINs, a family of variant surface proteins expressed on the surface of infected red blood cells, are able to directly bind LILRB1[49, 50]. K562 cells transfected with a LILRB1 binding RIFIN were more resistant to NK cell mediated lysis than those transfected with a RIFIN unable to bind LILRB1, suggesting that *Pf* RIFIN expression may play a role in immune evasion[43]. Whether CD56^{neg} NK cells bind *Pf*-RIFIN, and whether this regulates their subsequent activation, remains to be determined.

Along with a reduced response to cytokine stimulation, higher frequencies of CD56^{neg} NK cells were associated with a higher probability of being asymptomatic when subsequently infected with malaria parasites, independent of age and household level transmission intensity. In contrast, CD56^{dim} NK cells were much more inflammatory *in vitro*, and higher frequencies of these cells were associated with a higher probability of symptoms given infection. Given the age dependent inversion of the circulating CD56^{dim} to CD56^{neg} ratio among children living in a high malaria transmission setting, these data are consistent with the hypothesis that epigenetic and transcriptional regulation of the NK cell response is important in limiting the negative consequences of inflammation due to repeated blood-stage malaria.

Despite this reduced response to cytokine stimulation, we observed that CD56^{neg} NK cells potently degranulate in response to opsonized iRBC, and were able to mediate killing of opsonized p815 cells, consistent with a role for these cells having a specialized capacity to

perform ADCC. Higher percentages of these cells were also associated with lower parasite densities upon subsequent infection, suggesting an important role of these cells *in vivo* in mediating anti-parasite immunity. Our data are similar to recently described $CD56^{dim}$ adaptive NK cells, also characterized by low PLZF and FcRγ expression, which were found to have enhanced ADCC against *Pf* infected red blood cells and were associated with protection against incident malaria[25]. That study identified NK cells based on CD56 expression and therefore excluded $CD56^{neg}$ NK cells. Given their similar phenotype and function to the $CD56^{neg}$ cells we describe, we suspect significant overlap between adaptive, $PLZF^{low}$ /$FcR\gamma^{low}$ $CD56^{dim}$ and $CD56^{neg}$ NK cell subsets.

Importantly, we show that higher percentages of $CD56^{neg}$ NK cells were higher in children with greater *Pf* exposure, and that, following a marked reduction in malaria transmission, both the frequency and function of these cells declines rapidly. Together, these data strongly suggest that continuous exposure to malaria is required to maintain circulating frequencies of $CD56^{neg}$ NK cells. It remains to be determined whether and how malaria drives expansion of these cells, and whether these cells represent a clonal, "terminally differentiated" population of NK cells vs. expansion of a unique NK cell subset. In contrast to CMV infection, where virally encoded peptides induce expansion of CMV-specific, NKG2C-expressing adaptive NK cells[51], our *in vitro* data do not suggest that $CD56^{neg}$ NK cells respond directly to *Pf* stimulation. Nonetheless, their heightened malaria-specific and non-specific (e.g. P815 cell) antibody-depedent functionality suggests that these cells play a critical role in innate/adaptive immune bridging.

There were limitations in this study. Not all assays could be performed on all subjects due to sample availability and cost. However, this remains a comprehensive study, leveraging the infrastructure of the East African ICEMR with longitudinal sampling in multiple subjects. Despite

their phenotypic, transcriptional, and functional similarity to other NK cells, the ontology of these cells remains unclear, and it remains possible that CD56^{neg} NK cells may be better classified as an alternative innate lymphoid cell (ILC) subset[52]. Additional functional characterization of these cells is ongoing. Epidemiological analyses are limited to associations with measure of clinical immunity conditional on participants being infected (i.e. microscopic parasite densities or symptoms if infected). This study is unable to determine whether NK cell subsets are associated developing a blood stage infection in the first place, nor whether these subsets are associated with protection against sub-microscopic parasitemia. Although our data strongly suggest that repeated exposure to malaria results in increased frequencies of CD56^{neg} NK cells, we cannot exclude the possibility that other infections may drive expansion of these cells in this setting. Nearly all children were CMV seropositive at the time of sampling, precluding comparisons between CMV seropositive and CMV seronegative children, and though subjects were not tested for EBV, the prevalence of EBV in similar East African settings has been noted to be very high early in life[53]. Furthermore, associations between aEIR and NK cell phenotypes, and declining percentages of CD56^{neg} NK cells in children following interruptions in malaria transmission, strongly implicate the need for repeated exposure to drive higher frequencies of these cells. Finally, given the low number of infections following IRS initiation, we were not able to determine whether this immunologic change was associated with a higher propensity for either symptomatic and/or high parasite density infections.

By showing that adaptive-like, functional CD56^{neg} NK cells are associated with anti-disease and anti-parasite protection against malaria, we have identified a new role of NK cells in malaria-endemic settings. Understanding factors that drive programming of this unique NK cell subset will help therapeutic translation, including enhancing vaccine-elicited protection. Our findings that these cells are lost in the absence of continuous malaria exposure has important implications regarding maintenance of clinical immunity following interruptions in malaria

transmission. It is generally presumed that clinical immunity to malaria is short-lived and wanes rapidly[3], due in part to selective and rapid loss of malaria-specific antibodies[54]. To our knowledge, selective and rapid loss of a cellular correlate of protection following interruptions in malaria transmission has not been described, and understanding whether this loss plays a role in resurgence and/or delayed malaria following withdrawal of effective malaria control interventions remains to be determined[55]. Finally, as higher frequencies of $CD56^{neg}$ NK cells have been implicated in the pathogenesis of malignancies including Burkitt's Lymphoma[29] and AML[28], understanding the impact of these malaria-induced NK cell changes on immune surveillance of malignancy, and responses to other infectious diseases and/or vaccinations, remains critically important.

Acknowledgments

We are grateful to all the parents and guardians for giving their consent and to the study participants for their cooperation. We thank all the members of the study team for their tireless effort and excellent work. **Funding:** Support for this work was provided by the Bill and Melinda Gates Foundation/Stanford Center for Human Systems Immunology (Pilot Project to PJ), NIH/NIAID U01AI150741 (ZH, ST, IRB, BG, and PJ), R01AI093615 (MEF), NIH/NIAID U19AI089674 (GD) **Author contributions:** MT designed, performed, and analyzed most experiments with assistance from KDP, KvdP, JN, S.Tu., LdP, MB, and PJ and drafted the manuscript. SS and ZH analyzed cite-seq experiments described in Fig 2 and edited the manuscript. PC and M.E.F. performed analysis as related to figure 3C and edited the manuscript. JR and EA coordinated clinical study, provided patient care and collected patient data. F.N., K.M., and I.S. coordinated, collected and processed patient samples for all experiments. KDP, SK, and WG conducted ATAC-Seq analysis reported in Figure 6d. JN, PU, PK conducted EpiTOF analysis reported in Fig 4E. IRB, BG, and CB provided critical input into

experimental design, interpretation of results, and edited the manuscript. GD developed, funded, and coordinated the clinical study, and analyzed data related to Fig 6a. MK developed, funded, and coordinated the clinical study. M.E.F. provided participant samples for analysis. PJ designed and coordinated the project, evaluated the data, provided funding for all experiments, and prepared the manuscript. All authors reviewed and approved the manuscript. **Competing interests:** The authors declare that they have no competing interests. **Data and materials availability:** All raw data are available from the corresponding author upon request without restriction. RNA sequencing data have been deposited at NCBI Gene Expression Omnibus and are publicly available as of the date of publication.

Methods

Study site and participants

Samples were obtained from children followed longitudinally through the East African International Centres of Excellence in Malaria Research cohorts in Tororo and Jinja districts[56]. In these settings, malaria transmission is year-round, with two seasonal peaks and varied transmission intensities[31]. In Tororo District, before 2015, malaria control was limited to the distribution of LLINs, promotion of intermittent preventive treatment during pregnancy, and malaria case management with artemether lumefantrine. Indoor residual spraying with the carbamate bendiocarb was first initiated in December 2014–January 2015, with additional rounds administered in June 2015–July 2015 and November 2015–December 2015. In June 2016–July 2016, IRS was administered with the organophosphate pirimiphos-methyl (Actellic), with repeated rounds in June 2017–July 2017, June 2018–July 2018, and March 2019–April 2019. Initiation or IRS in Tororo district was accompanied by dramatic reductions in malaria transmission.

Children were followed for all care at a dedicated study clinic. Those who presented with a fever (tympanic temperature >38.0 °C) or history of fever in the previous 24 hours had blood obtained by finger prick for a thick smear. If the thick smear was positive for *Plasmodium* parasites, the patient was diagnosed with malaria regardless of parasite density, and treated with artemether-lumefantrine. Routine assessments were performed in the study clinic every month, including blood smears to detect for microscopic Pf parasitemia. Participants with asymptomatic parasitemia were not treated with antimalaria drugs in accordance with local guidelines. Household annualized entomologic inoculation rates (aEIR) in the year prior to sampling were estimated from monthly Centers for Disease Control and Prevention (CDC) light trap mosquito collections. The aEIR was the product of the annual human biting rate (total number of female Anopheles mosquitoes captured/number of house nights of collection X 365 days/year) and the

sporozoite rate (number of mosquitoes testing positive for *Pf* sporozoites/number of mosquitoes tested). CMV serostatus was measured using Human Anti-Cytomegalovirus IgG ELISA Kit (CMV) ab108724. Nearly all children (98%) in this cohort were HCMV positive (**Supplemental Table 2**).

Written informed consent was obtained from the parent or guardian of all study participants. The study protocols were approved by the Uganda National Council of Science and Technology, the Makerere University School of Medicine Research and Ethics Committee, the University of California, San Francisco Committee on Human Research, and the Institutional Review Boards at Stanford University.

PBMC and Plasma Isolation

At select study visits, 3 to 10 mls of blood were obtained in acid citrate dextrose tubes and/or heparin tubes. Plasma was removed and peripheral blood mononuclear cells (PBMC) isolated by density gradient centrifugation (Ficoll-Histopaque; GE Life Sciences) were counted and cryopreserved in liquid nitrogen prior to shipping to our laboratories at Stanford for downstream analyses. Analysis of cell viability using Guava Viacount (Millipore) consistently demonstrated >90% viability after thaw. Plasma pooled from 12 adults followed in the high transmission Tororo district or from deidentified plasma from adult US donors was used in ADCC assays described below.

NK cell phenotyping

Thawed cells were allowed to rest at 37C for 5 hours before staining. After which, cells were washed with 1xPBS and surface antibodies were incubated at room temperature for 30 mins. Cells were washed with FACs buffer (1xPBS with 0.5% BSA and 0.5M EDTA) and fixed with

Thermo Fisher's Fix A for 15mins. Perm B (Thermo Fisher) was added to permeabilized cells along with intracellular antibodies and incubated for 20minutes at room temperature. Cells were washed by FACS buffer, then resuspended with 1x PBS before analysis on the Attune NXT flow cytometer. Data was analyzed with FlowJo X software (Tree Star). List of all antibodies can be found in Supplemental Table 2.

Epigenetic landscape profiling using cytometry by time of flight (EpiTOF)

Cryopreserved PBMCs were thawed and incubated in RPMI 1640 media (ThermoFisher) containing 10% FBS (ATCC) at 37°C for 1 hour prior to processing. Cisplatin (ENZO Life Sciences) was added to 10 mM final concentration for viability staining for 5 minutes before quenching with CyTOF Buffer (PBS (ThermoFisher) with 1% BSA (Sigma), 2mM EDTA (Fisher), 0.05% sodium azide). Cells were centrifuged at 400 g for 8 minutes and stained with lanthanide-labeled antibodies (Supplementary Table 7) against immunophenotypic markers in CyTOF buffer containing Fc receptor blocker (BioLegend) for 30 minutes at room temperature (RT). Following extracellular marker staining, cells were washed 3 times with CyTOF buffer and fixed in 1.6% PFA (Electron Microscopy Sciences) at $1x10^6$ cells/ml for 15 minutes at RT. Cells were centrifuged at 600 g for 5 minutes post-fixation and permeabilized with 1 mL ice-cold methanol (Fisher Scientific) for 20 minutes at 4_C. 4 mL of CyTOF buffer was added to stop permeabilization followed by 2 PBS washes. Mass-tag sample barcoding was performed following the manufacturer's protocol (Fluidigm). Individual samples were then combined and stained with intracellular antibodies in CyTOF buffer containing Fc receptor blocker (BioLegend) overnight at 4_C. The following day, cells were washed twice in CyTOF buffer and stained with 250 nM 191/193Ir DNA intercalator (Fluidigm) in PBS with 1.6% PFA for 30 minutes at RT. Cells were washed twice with CyTOF buffer and once with double-deionized water (ddH2O) (ThermoFisher) followed by filtering

through 35 mm strainer to remove aggregates. Cells were resuspended in ddH2O containing four element calibration beads (Fluidigm) and analyzed on CyTOF2 (Fluidigm).

CITE-Seq

The 10X Chromium platform was used to perform CITE-Seq. All protocols to generate scRNA-seq data on the 10x Chromium platform, including sample preparation, library preparation and instrument and sequencing settings, are available here: https://support.10xgenomics.com/single-cell-gene-expression

List of antibodies used for CITE-seq

Antibodies and clones used for Cite-Seq include (All anti-human TotalSeq B reagents, , USA): TBNK Cocktail, CD7 (CD7-6B7); TCR.Vd2 (B6); CD279 (EH12.2H7); HLADR (L243); CD123 (6H6); CD38 (HB-7); CD57 (QA17A04); CD370(8F9);CD1c (L161).See Supplementary Table for a list of antibodies, clones and barcodes used for CITE-seq.

Cell labeling with DNA-barcoded antibodies for CITE-seq

Approximately 1,000,000 cells from 10 patient samples were stained with Human TruStain FcX Fc Blocking Reagent (BioLegend, 422302) for 10 min at room temperature. The cells were stained for 30 min at 4 °C. Cells were then washed twice with PBS supplemented with 2% FCS and 2 mM EDTA (Sigma) before resuspending in PBS and counting. Approximately 10,000 cells per sample were loaded onto the 10x Chromium controller

CITE-seq on 10x platform

Gene expression libraries were prepared for each sample according to the manufacturer's protocol (10x Genomics). Cell-surface protein libraries were subjected to double the manufacturer's recommended primer concentration and seven to eight amplification cycles

during the sample index PCR to reduce the likelihood of daisy chains forming. All libraries were sequenced using a NovaSeq 6000 (Illumina) to achieve a minimum of 50,000 paired-end reads per cell for gene expression and 20,000 paired-end reads per cell for cell-surface protein libraries.

ATAC-Seq

To probe the epigenetic landscape, we used protocols and analysis software developed by the Greenleaf lab for Fast-ATAC (Corces et al. 2016)—a fast and sensitive version of ATAC-Seq (Buenrostro et al. 2015) requiring only 5000 cells and optimized for blood cells. This method uses hyperactive Tn5 transposase, which inserts sequencing adapters into chromatin-accessible regions. In brief, live $CD3^-CD14^-CD19^-CD7^+$ NK cells were sorted into FACS buffer and pelleted by centrifugation at 500g RCF at 4◦C in a pre-cooled fixed-angle centrifuge. The supernatant was removed carefully so as to not disturb the un-visible cell pellet. Fifty microliters of transposase mixture (25 ul of 2x TD buffer, 2.5 ul TDE1, 0.25 ul 2% digitonin, 22.5 ul nuclease-free water) was added to the cells. After mixing, samples were incubated at 37◦C for 30 min in an Eppendorf ThermoMixer with agitation at 300 rpm. Following this transposition reaction, the transposed DNA was purified using a QIAGEN MinElute Reaction Cleanup kit (28204) and purified DNA was eluted in 10 ul elution buffer (10mM Tris-HCl, pH 8). Transposed fragments were amplified and purified and libraries quantified using qPCR before sequencing. Fast-ATAC libraries were sequenced using paired-end, dual-index library sequencing on an Illumina NextSeq instrument (75bp kit, 36 base pair reads, ~20-30 million reads/sample).

Functional assays

Parasite Culture and Isolation

P. falciparum 3D7 asexual stage were cultured in RPMI 1640 with 25mM HEPES, 25mM sodium bicarbonate, 1% gentamycin, and enriched with 0.5% Albumax (pH 6.75) and 250uM hypoxanthine. The parasitemia was measured every other day by counting Giemsa (Sigma) stained blood smears, maintaining cultures at less than 10% parasitemia. Plates were kept at 37°C, under atmospheric conditions (5% oxygen, 5% carbon dioxide, and 95% nitrogen). To retain synchronous cultures, parasite growth was treated with 5% D-sorbitol, which lyses late-stage iRBCs leaving only ring stages. Schizont isolation was achieved using MACS cell separation LD columns (Miltenyi Biotec), and stored in -80°C. For experiments, schizonts were thawed, washed and resuspended in RPMI before addition to cells.

Mycoplasma contamination was assayed using the MycoAlert Mycoplasma Detection Kit (Lonza).

NK cell isolation

We used the Human NK Cell Isolation Kit (Miltenyi Biotec) to negatively isolate NK cells from freshly thawed PBMCs. First, cells were resuspended with buffer and mixed with NK cell biotin-antibody cocktail for 5 mins at 4C. Then, the provided NK Cell Microbead cocktail was added and incubated for 10mins at 4C. This was followed by magnetic cell separation using an LS column (Miltenyi Biotec). Flowthrough was collected, washed and resuspended in R10 (RPMI 1610 (Sigma) with 10% FBS (), 1%L-Glutamine (Thermo Fisher), 1% Penicillin and Gentamycin (Corning)).

Stimulation Assay

Thawed PBMC were rested for 1 hour at 37C before the addition of either uninfected RBCs, schizonts or cytokine cocktail containing 2.5ng/ml of recombinant human IL-12 (R&D systems), 10ng/ml of IL-15 (PeproTech) and 0.25ug of IL-18 (R&D systems). Cultures were incubated for 1 hour at 37C before addition of Protein Transport Inhibitor Brefeldin A (BD). Cells were kept at

37C for an additional 3 hours before staining and analysis on the Attune NXT flow cytometer. List of all antibodies can be found in Supplemental Table 2.

ADCC – Degranulation Assay

Freshly thawed schizonts were washed and incubated with RPMI, 10% pooled US plasma, 10% pooled immune Ugandan plasma or 1:100 anti-RBC (Abcam) at a concentration of 5x10^7 for 1 hour at 37C. Following opsonization, cells were washed and resuspended in R10 (see NK Isolation) before mixing with PBMCs or isolated NK cells. CD107a at a dilution of 1:250 (Clone H4A3, BioLegend) was immediately added with ER inhibitors – Monensin (BD Biosciences) and Protein Transport Inhibitor containing brefeldin A (BD Biosciences). Cells were spun for 3 mins at 100gs before incubating for 5 hours, after which cells were stained and analyzed using the Attune NXT flow cytometer. Data was analyzed with FlowJo X software (Tree Star). List of all antibodies can be found in Supplemental Table 2 and 3.

ADCC - p815 Killing Assay

Killing assay performed as previously described[57, 58] with some modifications. Briefly, p815 cells (a mouse leukemia line) were stained with CellTrace Violet Cell Proliferation Kit (ThermoFisher) at 37C for 20mins. Reaction was stopped by addition of RPMI (Corning) with 10% FBS at 37C for 5 mins. Stained p815 cells were either opsonized with 10ug/ml p815 rat anti-mouse antibody (Clone: 2.4G2, BD Biosciences) or left uncoated for 30mins at 37C. After incubation, PBMCs were cocultured with opsonized and uncoated target cells at an effector:target ratio of 10:1. Co-cultures were incubated at 37C for 5 hours, before staining for dead and dying cells using 7-AAD Viability staining solution (1:25, Biolegend) and PE Annexin V (1:20, Biosciences) in 1x BD Annexin V Binding Buffer for 15mins at room temperature. Volume was brought up to 200ul and analyzed on the Attune NXT Flow Cytometer within the hour and analyzed with FlowJo X (Tree Star) software. Percentage of killed target cells was calculated by subtracting the percentages of dead uncoated target cells from the percentages of dead opsonized target cells.

Statistical analysis

All statistical analyses were performed using STATA version 16 (College Station), SPICE v.5.3 (NIAID), Prism 9.0 (GraphPad), or R version 4.2.0. Comparisons of cellular percentages between groups were performed using the Wilcoxon rank sum and/or *t* test, and the Wilcoxon signed-rank and/or paired *t* test was used to compare paired data. Associations between continuous variables were assessed using Spearman's rank correlation (ρ). Dimensionality reduction was performed with Uniform Manifold Approximation and Projection (UMAP)[59]. Associations between NK cell tertiles and the monthly probability of symptoms if parasitemic (detected by microscopy), and geometric mean parasite densities if parasitemic, were evaluated using multilevel mixed-effects models. These analyses accounted for repeated measures within individuals and were clustered on household to account for multiple children living in the same household. In multivariate analyses, odds ratios for symptoms when infected were adjusted for age and aEIR. Two-sided p-values were calculated for all test statistics and $P < 0.05$ was considered significant.

Cite-Seq Analysis

Droplet libraries were processed using Cell Ranger v4.0. Reads were aligned to the GRCh38 human genome using STAR (v2.5.1b) and unique molecular identifiers (UMIs) deduplicated. Antibody-derived tag (ADT) counts for each protein were first normalized using counts per million and log transformed, with a pseudocount of +1. To estimate the background signal for each protein, a two-component Gaussian mixture model, implemented in the R package function 'mclust' (v5.4.7), was fit across the droplets with a total UMI count of >10 and <100 from each experimental sample separately. The mean of the first Gaussian mixture model component for each protein was then subtracted from the log counts per million from the QC-passed droplets in the respective experimental sample. Raw data was filtered to remove cells that expressed fewer than 200 genes and >10% mitochondrial reads. We used the variable

stabilization transformation (VST) from the Seurat R package[60] to integrate and transform the count data into normalized and scaled data that can be used for downstream analysis.

We used Uniform Manifold Approximation and Projection (UMAP) for dimensionality reduction and data visualization. We used the Louvain algorithm to identify cell clusters. We used the singleR[61] package to annotate the cell clusters by comparing the transcriptomics profile between the cell clusters and reference data from Human Primary Cell Atlas[62]. We manually gated the protein-level expression data to identify the three NK cell subsets, including CD56- NK cells (CD19- CD3- CD14- CD7+ CD16+ CD56-), $CD56^{dim}$ NK cells (CD19- CD3- CD14- CD7+ CD16+ $CD56^{dim}$) and CD56+ NK cells (CD19- CD3- CD14- CD7+ CD16- CD56+). The identified cells were mapped to the UMAP to confirm their identity as NK cells based on transcriptomics profiles. We performed likelihood ratio tests (implemented as the FindMarkers function in the Seurat R package[60]) to identify differentially expressed genes between CD56- NK cells and $CD56^{dim}$ NK cells.

EpiTOF Analysis

Raw data were pre-processed using FlowJo (FlowJo, LLC) to identify cell events from individual samples by palladium-based mass tags, and to segregate specific immune cell populations by immunophenotypic markers. A detailed gating hierarchy is described in Supplemental Figure 3 . Single-cell data for various immune cell subtypes from individual subjects were exported from FlowJo for downstream computational analyses.

The exported Flowjo data were then normalized following previously reported methods[42]. In brief, the value of each histone mark was regressed against the total amount of histones, represented by measured values of H3 and H4. For sample level analyses, the values of each

histone mark were averaged for each cell type in each sample. Distances of HSC from lymphoid and myeloid epigenetic profiles were obtained by first computing centers of the epigenetic profiles for the two lineages, and then computing Euclidean distances from the centers for each individual HSC. Distances of HSC from epigenetic profiles of specific cell types were similarly obtained by computing Euclidean distances from the centers of the epigenetic profiles for each cell type. Statistical significance of the differences between groups at the sample level was assessed by computing an effect size with Hedges' g formula[63]. All p-values were corrected for multiple comparisons with the Benjamini-Hochberg method[64].

ATAC-Seq Analysis

We used ChrAccR, an R package for comprehensive analysis of chromatin accessibility data (https://greenleaflab.github.io/ChrAccR/). This program uses DESeq2 (Love et al. 2014) for differential accessible peak calling, ChromVAR[65] for differential motif calling, and LOLA[66] for peak enrichment analysis. We identified open chromatin peaks that varied across the different timepoints from the same child and that are differentially enriched for transcription factor binding motifs in regulatory elements (e.g. gene promoters and distal enhancers). Specific sites of interest visualized with Integrative Genome Viewer (Broad Institute, Cambridge, MA).

References

1. Organization, W.H. World malaria report 2021. (2021).

2. Rodriguez-Barraquer, I. *et al.* Quantification of anti-parasite and anti-disease immunity to malaria as a function of age and exposure. *Elife* **7** (2018).

3. Langhorne, J., Ndungu, F.M., Sponaas, A.M. & Marsh, K. Immunity to malaria: more questions than answers. *Nat Immunol* **9**, 725-732 (2008).

4. Tan, J., Piccoli, L. & Lanzavecchia, A. The Antibody Response to Plasmodium falciparum: Cues for Vaccine Design and the Discovery of Receptor-Based Antibodies. *Annu. Rev. Immunol.* (2018).

5. Reiling, L. *et al.* Targets of complement-fixing antibodies in protective immunity against malaria in children. *Nat Commun* **10**, 610 (2019).

6. Osier, F.H. *et al.* Opsonic phagocytosis of Plasmodium falciparum merozoites: mechanism in human immunity and a correlate of protection against malaria. *BMC Med.* **12**, 108 (2014).

7. Boyle, M.J. *et al.* Human antibodies fix complement to inhibit Plasmodium falciparum invasion of erythrocytes and are associated with protection against malaria. *Immunity* **42**, 580-590 (2015).

8. Arora, G. *et al.* NK cells inhibit Plasmodium falciparum growth in red blood cells via antibody-dependent cellular cytotoxicity. *Elife* **7** (2018).

9. Stevenson, M.M. & Riley, E.M. Innate immunity to malaria. *Nat Rev Immunol* **4**, 169-180 (2004).

10. Stanisic, D.I. *et al.* gammadelta T cells and CD14+ monocytes are predominant cellular sources of cytokines and chemokines associated with severe malaria. *J Infect Dis* **210**, 295-305 (2014).

11. Chua, C.L., Brown, G., Hamilton, J.A., Rogerson, S. & Boeuf, P. Monocytes and macrophages in malaria: protection or pathology? *Trends Parasitol* **29**, 26-34 (2013).

12. Riley, E.M. *et al.* Immune response to soluble exoantigens of Plasmodium falciparum may contribute to both pathogenesis and protection in clinical malaria: evidence from a longitudinal, prospective study of semi-immune African children. *Eur J Immunol* **21**, 1019-1025 (1991).

13. Jagannathan, P. *et al.* Loss and dysfunction of Vdelta2(+) gammadelta T cells are associated with clinical tolerance to malaria. *Sci Transl Med* **6**, 251ra117 (2014).

14. Jagannathan, P. *et al.* Vdelta2+ T cell response to malaria correlates with protection from infection but is attenuated with repeated exposure. *Sci Rep* **7**, 11487 (2017).

15. Guha, R. *et al.* Plasmodium falciparum malaria drives epigenetic reprogramming of human monocytes toward a regulatory phenotype. *PLoS Pathog* **17**, e1009430 (2021).

16. Farrington, L.A. *et al.* Opsonized antigen activates Vdelta2+ T cells via CD16/FCgammaRIIIa in individuals with chronic malaria exposure. *PLoS Pathog* **16**, e1008997 (2020).

17. von Borstel, A. *et al.* Repeated Plasmodium falciparum infection in humans drives the clonal expansion of an adaptive gammadelta T cell repertoire. *Sci Transl Med* **13**, eabe7430 (2021).

18. Dobbs, K.R. *et al.* Monocyte dysregulation and systemic inflammation during pediatric falciparum malaria. *JCI Insight* **2** (2017).

19. Artavanis-Tsakonas, K. & Riley, E.M. Innate immune response to malaria: rapid induction of IFN-gamma from human NK cells by live Plasmodium falciparum-infected erythrocytes. *J Immunol* **169**, 2956-2963 (2002).

20. Artavanis-Tsakonas, K. *et al.* Activation of a subset of human NK cells upon contact with Plasmodium falciparum-infected erythrocytes. *J Immunol* **171**, 5396-5405 (2003).

21. Wolf, A.S., Sherratt, S. & Riley, E.M. NK Cells: Uncertain Allies against Malaria. *Front Immunol* **8**, 212 (2017).

22. Horowitz, A. *et al.* Genetic and environmental determinants of human NK cell diversity revealed by mass cytometry. *Sci Transl Med* **5**, 208ra145 (2013).

23. Strauss-Albee, D.M. *et al.* Human NK cell repertoire diversity reflects immune experience and correlates with viral susceptibility. *Sci Transl Med* **7**, 297ra115 (2015).

24. Yang, C. *et al.* Heterogeneity of human bone marrow and blood natural killer cells defined by single-cell transcriptome. *Nat Commun* **10**, 3931 (2019).

25. Hart, G.T. *et al.* Adaptive NK cells in people exposed to Plasmodium falciparum correlate with protection from malaria. *J Exp Med* **216**, 1280-1290 (2019).

26. Mavilio, D. *et al.* Characterization of CD56-/CD16+ natural killer (NK) cells: a highly dysfunctional NK subset expanded in HIV-infected viremic individuals. *Proc Natl Acad Sci U S A* **102**, 2886-2891 (2005).

27. Gonzalez, V.D. *et al.* Expansion of functionally skewed CD56-negative NK cells in chronic hepatitis C virus infection: correlation with outcome of pegylated IFN-alpha and ribavirin treatment. *J Immunol* **183**, 6612-6618 (2009).

28. Chretien, A.S. *et al.* High-dimensional mass cytometry analysis of NK cell alterations in AML identifies a subgroup with adverse clinical outcome. *Proc Natl Acad Sci U S A* **118** (2021).

29. Forconi, C.S. *et al.* Poorly cytotoxic terminally differentiated CD56(neg)CD16(pos) NK cells accumulate in Kenyan children with Burkitt lymphomas. *Blood Adv* **2**, 1101-1114 (2018).

30. Bjorkstrom, N.K., Ljunggren, H.G. & Sandberg, J.K. CD56 negative NK cells: origin, function, and role in chronic viral disease. *Trends Immunol* **31**, 401-406 (2010).

31. Kamya, M.R. *et al.* Malaria transmission, infection, and disease at three sites with varied transmission intensity in Uganda: implications for malaria control. *Am J Trop Med Hyg* **92**, 903-912 (2015).

32. Holmes, T.D. *et al.* The transcription factor Bcl11b promotes both canonical and adaptive NK cell differentiation. *Sci Immunol* **6** (2021).

33. Brownlie, D. *et al.* Expansions of adaptive-like NK cells with a tissue-resident phenotype in human lung and blood. *Proc Natl Acad Sci U S A* **118** (2021).

34. Born, T.L., Thomassen, E., Bird, T.A. & Sims, J.E. Cloning of a novel receptor subunit, AcPL, required for interleukin-18 signaling. *J Biol Chem* **273**, 29445-29450 (1998).

35. Narayanan, S. *et al.* LAG3 is a Central Regulator of NK Cell Cytokine Production. *bioRxiv*, 2020.2001.2031.928200 (2020).

36. Merino, A. *et al.* Chronic stimulation drives human NK cell dysfunction and epigenetic reprograming. *J Clin Invest* **129**, 3770-3785 (2019).

37. Anderson, A.C., Joller, N. & Kuchroo, V.K. Lag-3, Tim-3, and TIGIT: Co-inhibitory Receptors with Specialized Functions in Immune Regulation. *Immunity* **44**, 989-1004 (2016).

38. Smith, S.L. *et al.* Diversity of peripheral blood human NK cells identified by single-cell RNA sequencing. *Blood Adv* **4**, 1388-1406 (2020).

39. Bjorkstrom, N.K. *et al.* Expression patterns of NKG2A, KIR, and CD57 define a process of CD56dim NK-cell differentiation uncoupled from NK-cell education. *Blood* **116**, 3853-3864 (2010).

40. Schlums, H. *et al.* Cytomegalovirus infection drives adaptive epigenetic diversification of NK cells with altered signaling and effector function. *Immunity* **42**, 443-456 (2015).

41. Digitale, J.C. *et al.* Association of Inhibitory Killer Cell Immunoglobulin-like Receptor Ligands With Higher Plasmodium falciparum Parasite Prevalence. *J Infect Dis* **224**, 175-183 (2021).

42. Cheung, P. *et al.* Single-Cell Chromatin Modification Profiling Reveals Increased Epigenetic Variations with Aging. *Cell* **173**, 1385-1397 e1314 (2018).

43. Cruz, C. *et al.* Tri-methylation of histone H3 lysine 4 facilitates gene expression in ageing cells. *Elife* **7** (2018).

44. Hwang, I. *et al.* Identification of human NK cells that are deficient for signaling adaptor FcRgamma and specialized for antibody-dependent immune functions. *Int Immunol* **24**, 793-802 (2012).

45. Nankabirwa, J.I. *et al.* Malaria Transmission, Infection, and Disease following Sustained Indoor Residual Spraying of Insecticide in Tororo, Uganda. *Am J Trop Med Hyg* **103**, 1525-1533 (2020).

46. Caligiuri, M.A. Human natural killer cells. *Blood* **112**, 461-469 (2008).

47. Milush, J.M. *et al.* Functionally distinct subsets of human NK cells and monocyte/DC-like cells identified by coexpression of CD56, CD7, and CD4. *Blood* **114**, 4823-4831 (2009).

48. Milush, J.M. *et al.* CD56negCD16(+) NK cells are activated mature NK cells with impaired effector function during HIV-1 infection. *Retrovirology* **10**, 158 (2013).

49. Saito, F. *et al.* Immune evasion of Plasmodium falciparum by RIFIN via inhibitory receptors. *Nature* **552**, 101-105 (2017).

50. Chen, Y. *et al.* Structural basis of malaria RIFIN binding by LILRB1-containing antibodies. *Nature* **592**, 639-643 (2021).

51. Hammer, Q. *et al.* Peptide-specific recognition of human cytomegalovirus strains controls adaptive natural killer cells. *Nat Immunol* **19**, 453-463 (2018).

52. Simoni, Y. *et al.* Human Innate Lymphoid Cell Subsets Possess Tissue-Type Based Heterogeneity in Phenotype and Frequency. *Immunity* **46**, 148-161 (2017).

53. Piriou, E. *et al.* Early age at time of primary Epstein-Barr virus infection results in poorly controlled viral infection in infants from Western Kenya: clues to the etiology of endemic Burkitt lymphoma. *J Infect Dis* **205**, 906-913 (2012).

54. Ssewanyana, I. *et al.* Impact of a Rapid Decline in Malaria Transmission on Antimalarial IgG Subclasses and Avidity. *Front Immunol* **11**, 576663 (2020).

55. Greenwood, B. *et al.* Resurgent and delayed malaria. *Malar J* **21**, 77 (2022).

56. Zehner, N. *et al.* Age-Related Changes in Malaria Clinical Phenotypes During Infancy Are Modified by Sickle Cell Trait. *Clin Infect Dis* **73**, 1887-1895 (2021).

57. Roy Chowdhury, R. *et al.* A multi-cohort study of the immune factors associated with M. tuberculosis infection outcomes. *Nature* **560**, 644-648 (2018).

58. Salinas-Jazmín, N., Hisaki-Itaya, E. & Velasco-Velázquez, M.A. A flow cytometry-based assay for the evaluation of antibody-dependent cell-mediated cytotoxicity (ADCC) in cancer cells. *Methods Mol Biol* **1165**, 241-252 (2014).

59. McInnes, L., Healy, J. & Melville, J. UMAP: uniform manifold approximation and projection for dimension reduction. (2020).

60. Hao, Y. *et al.* Integrated analysis of multimodal single-cell data. *Cell* **184**, 3573-3587 e3529 (2021).

61. Aran, D. *et al.* Reference-based analysis of lung single-cell sequencing reveals a transitional profibrotic macrophage. *Nat Immunol* **20**, 163-172 (2019).

62. Mabbott, N.A., Baillie, J.K., Brown, H., Freeman, T.C. & Hume, D.A. An expression atlas of human primary cells: inference of gene function from coexpression networks. *BMC Genomics* **14**, 632 (2013).

63. Hedges, L.V. & Olkin, I. *Statistical methods for meta-analysis*. Academic press, 2014.

64. Benjamini, Y. & Hochberg, Y. Controlling the false discovery rate: a practical and powerful approach to multiple testing. *Journal of the Royal statistical society: series B (Methodological)* **57**, 289-300 (1995).

65. Schep, A.N., Wu, B., Buenrostro, J.D. & Greenleaf, W.J. chromVAR: inferring transcription-factor-associated accessibility from single-cell epigenomic data. *Nat Methods* **14**, 975-978 (2017).

66. Sheffield, N.C. & Bock, C. LOLA: enrichment analysis for genomic region sets and regulatory elements in R and Bioconductor. *Bioinformatics* **32**, 587-589 (2016).

Supplementary Files

This is a list of supplementary files associated with this preprint. Click to download.

- NKPaperSupplementary.docx
- SupplementalTable.csv